Cu(II) Carboxylate Arene C–H Functionalization: Tuning for Non-Radical Pathways

Authors

Fanji Kong[1], Shusen Chen[2], Junqi Chen[1], Chang Liu[1], Weihao Zhu[1], Diane A. Dickie[1], William L. Schinski[3], Sen Zhang[1], Daniel H. Ess[2]* and T. Brent Gunnoe[1]*

Affiliations

[1]Department of Chemistry, University of Virginia; Charlottesville, Virginia 22904, United States.

[2]Department of Chemistry and Biochemistry, Brigham Young University; Provo, Utah 84604, United States.

[3]Retired. Consulting scientist, San Rafael, California 94903, United States.

*Corresponding author. Email: tbg7h@virginia.edu

*Corresponding author for computational studies. Email: dhe@chem.byu.edu

Abstract

We report C–H acetoxylation of non-directed arenes benzene and toluene, as well as related functionalization with OPiv and OHex ester groups (OPiv = pivalate; OHex = 2-ethylhexanoate), using simple Cu(II) salts with over 80% yield. By changing the ratio of benzene and Cu(II) salts, 2.4% conversion of benzene can be reached. Combined experimental and computational studies results indicate that the arene C–H functionalization likely occurs by a non-radical Cu(II)-mediated organometallic pathway. The Cu(II) salts used in the reaction can be isolated, recycled, and reused with little change in reactivity. Also, the Cu(II) salts can be regenerated *in situ* using O_2 and, after the removal of the generated water, the arene C–H acetoxylation and related esterification reactions can be continued, which leads to a process that enables recycling of Cu(II).

Teaser

The C–H acetoxylation of benzene or toluene using air-recyclable Cu(II) salts through a non-radical organometallic pathway is reported.

Introduction

As an important industrial chemical, phenol has been deployed in applications in various fields including household products, nylon, polymers, and the manufacturing of other chemical derivatives. Over 12 million tonnes of phenol are produced each year, and greater than 90% of phenol is produced through the Hock process (*1-2*). However, a major issue with the Hock process is the generation of a stoichiometric amount of acetone as an oversupplied side product (*1*). Alternative methods for phenol production include a three-step route from benzene to phenol with cyclohexanone as a coproduct developed by ExxonMobil, and the oxidation of benzene using N_2O developed by Solutia (*3-5*). However, the source of N_2O gas limits the location and amount of phenol production for the Solutia process, while neither of the other methods provide a desirable coproduct-free route for phenol production (**Figure 1**). Other related benzene hydroxylation processes using copper rely on the formation of hydroxyl radical and/or requires solid-supports to form heterogeneous catalysts (*2,6-8*), which suffer from low selectivity and/or low yield.

Acetoxylation of benzene has been considered as a potential route for phenol production since hydrolysis of phenyl acetate generates phenol (*9*). Palladium-catalyzed benzene acetoxylation has been studied (*10-11*), but only a limited number of examples of aromatic C–H acetoxylation/hydroxylation have been reported using low-cost transition metals, and these examples rely on functionalized aromatic substrates with "directing groups" to facilitate coordination to the catalyst (*12-19*). Yu and co-workers demonstrated a series of C–H functionalizations using pyridine as the directing group with copper(II) acetate as the catalyst precursor, and the reaction was proposed to occur by the formation of a radical cation intermediate via a single electron transfer (SET) mechanism (*12*). Later, the Shi group reported a study using a bidentate directing group derived from 2-(pyridine-2-yl)isopropylamine through a proposed Cu(III)–aryl intermediate (*13*). Subsequently, the Yu group demonstrated a related C–H hydroxylation process using oxazolyamide as the directing group via a possible monomeric Cu(III)–aryl intermediate (*15*). Benzoic acid has also been reported as a directing group for the synthesis of hydroxylated arenes assisted by benzoyl peroxide (*17*). Other related C–H functionalization processes by Cu(II) also require a directing group to facilitate the reaction (*20-31*).

To our knowledge there are no reported examples of molecular Cu(II)-mediated arene acetoxylation without directing groups on the arene. Herein, we report acetoxylation of benzene and toluene using simple Cu(II) salts, and we propose that the C–H functionalization occurs by a non-radical organometallic pathway that forms Cu–aryl intermediates under certain conditions. The Cu(II) salt offers recyclability using O_2 or air, similar to the commercialized Pd-catalyzed ethylene oxidation Wacker process that has proven viable with Cu(II) recycling both *in situ* (with purified O_2) and in a separate step/reactor from the ethylene oxidation process (using air) (*32-35*). This process can potentially lead to a coproduct-free synthetic route for phenol production (**Figure 1**), since all of the coproducts are used for recycling of the Cu(II) salt, and thus the overall reaction is the conversion of benzene and dioxygen to phenol (**Figure 1**).

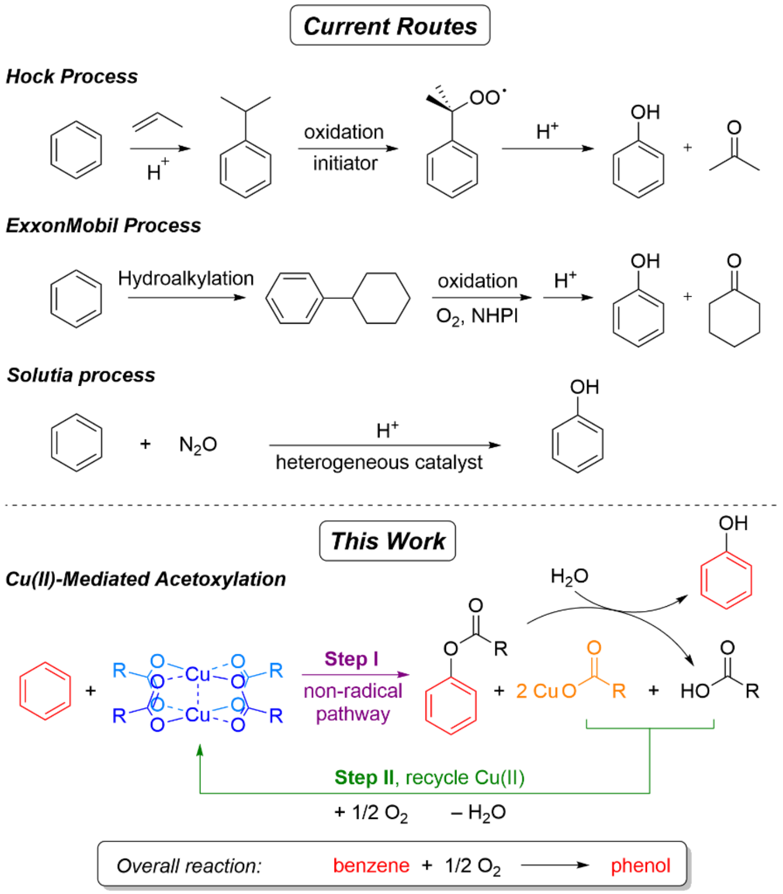

Figure 1. Current methods for phenol production and the proposed method via Cu(II)-mediated acetoxylation (NHPI = *N*-hydroxyphthalimide).

Results

Development of non-directed Cu(II)-mediated C–H acetoxylation of benzene. Phenyl acetate has been observed as a side product in our previously reported Rh catalyzed arene alkenylation that incorporates $Cu(OAc)_2$. Phenyl acetate formation is the result of a reaction of $Cu(OAc)_2$ with benzene (*36*). After initial optimization of conditions (Supplementary Materials, Sections 2 and 3), we found that heating (180 °C) 10 mL of a benzene mixture with pre-dried $Cu(OAc)_2$ (0.48 mol% relative to benzene) under dinitrogen (75 psig) produces phenyl acetate in 87(1)% yield based on the Cu(II) limiting reagent as determined by GC-FID (**Table 1**, entry 2). The control experiment using $CuCl_2$ showed no activity for C–H activation on benzene (**Table 1**, entry 12), which likely indicates the carboxylate group is essential for arene C–H activation (see below). Similar to $Cu(OAc)_2$, more soluble Cu(II) salts, such as Cu(II) pivalate ($Cu(OPiv)_2$) and Cu(II) 2-ethylhexanoate ($Cu(OHex)_2$), were shown to achieve similar reactions at even a lower temperature (**Table 1**, entries 6, 7 and 9). The Cu(II) species $Cu(OPiv)_2$ was found to give a lower yield compared to the other Cu(II) salts, which we attribute to the lower thermostability of the pivalic group (Supplementary Materials, Section 2.5). The presence of air was found to inhibit the reaction (**Table 1**, entry 4), and the reaction was slowed down with the addition of an increasing amount of carboxylic acid (**Table 1**, entries 3, 5, 8, 10, 11). Different ligands and solvents were tested for the reaction; however, none of them provided a beneficial effect (Supplementary Materials, Sections 5.1 and 6). These observations are distinct from the previously published directed Cu(II)-mediated acetoxylation processes (*12,14-19*), in which the presence of acid, air or ligands are commonly required by the reactions.

Table 1. Selected results for benzene acetoxylation and related reactions using Cu(II) salts. Yield of the phenyl carboxylate is relative to the limiting reagent (CuX_2) as determined by GC-FID. The theoretical maximum conversion of benzene will be 0.24%. Reaction conditions: benzene (10 mL, 112.3 mmol), CuX_2 (0.48 mol%, 0.540 mmol), 75 psig N_2. CuX_2 = $Cu(OAc)_2$ anhydrous; $Cu(OPiv)_2$, or $Cu(OHex)_2$. N.D. = not detected. Standard deviations were calculated from at least three independent experiments.

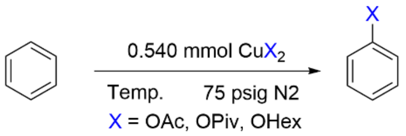

Entry	Cu(II) salt	Temp. (°C)	HX (equiv.)	Air	Yield (%)	Time (h)
1	$Cu(OAc)_2$	180	0	none	78(0)	24
2	$Cu(OAc)_2$	180	0	none	87(1)	40
3	$Cu(OAc)_2$	180	1.0	none	80(1)	40
4[a]	$Cu(OAc)_2$	180	0	1 atm.	15(2)	24
5	$Cu(OAc)_2$	180	4.0	none	65(6)	48
6	$Cu(OPiv)_2$	180	0	none	49(1)	16
7	$Cu(OPiv)_2$	170	0	none	52(0)	16
8	$Cu(OPiv)_2$	170	1.0	none	36(1)	16
9	$Cu(OHex)_2$	170	0	none	89(1)	24
10	$Cu(OHex)_2$	170	1.0	none	71(1)	40
11	$Cu(OHex)_2$	170	4.0	none	37(0)	72
12[b]	$CuCl_2$	180	0	none	N.D.	24

[a] Using 1 atm of air, the total top pressure of air and N_2 is 75 psig. [b] Using half the amount of reagents in a VCO reactor under 100 psig Ar.

Mechanistic studies. To differentiate between radical and non-radical pathways, separate reactions of toluene or a mixture of benzene with cyclohexane were used as probes. These reactions offer intramolecular and intermolecular competition of weaker sp^3 C–H bonds and stronger sp^2 C–H bonds (**Figure 2, A** and **B**). It is expected that a radical C–H abstraction reaction will select for the weaker sp^3 C–H bonds. Under anhydrous conditions, all of the reactions were found to select for the stronger sp^2 C–H bonds, which suggests that the reactions likely undergo a non-radical reaction pathway. Using 1 mL of benzene with 9 mL of cyclohexane resulted in ~10% of the rate compared to the reaction using neat benzene, consistent with the reaction being first-order in benzene. A common radical trap, (2,2,6,6-tetramethylpiperidin-1-yl)oxyl (TEMPO), was tested as an additive in the reaction of toluene with $Cu(OAc)_2$ (**Figure 2C**). The reactions with TEMPO were slow and remained selective for tolyl acetates, but more benzyl acetate was formed compared to reactions without TEMPO. In a control experiment, we found that TEMPO can functionalize the benzylic position of toluene without Cu(II) salt (**Figure 2D**). When using toluene as the substrate, the regioselectivity of the sp^2 C–H bonds can be used to differentiate between a potential electrophilic aromatic substitution mechanism ($^{Ar}S_E$, with no M−C bond formation), and a metal-mediated C−H activation mechanism via M−C bond formation (*37-38*). The Cu(II) mediated reaction was found to be more selective for the meta-tolyl carboxylate than the ortho-tolyl carboxylate (**Table 2**, entries 1, 4 and 5), which we propose (see below) is a result of an organometallic reaction that forms Cu–tolyl intermediates. We propose that the Cu-mediated toluene C–H activation favors the meta- over the ortho-position of toluene due to the steric effect of the methyl group.

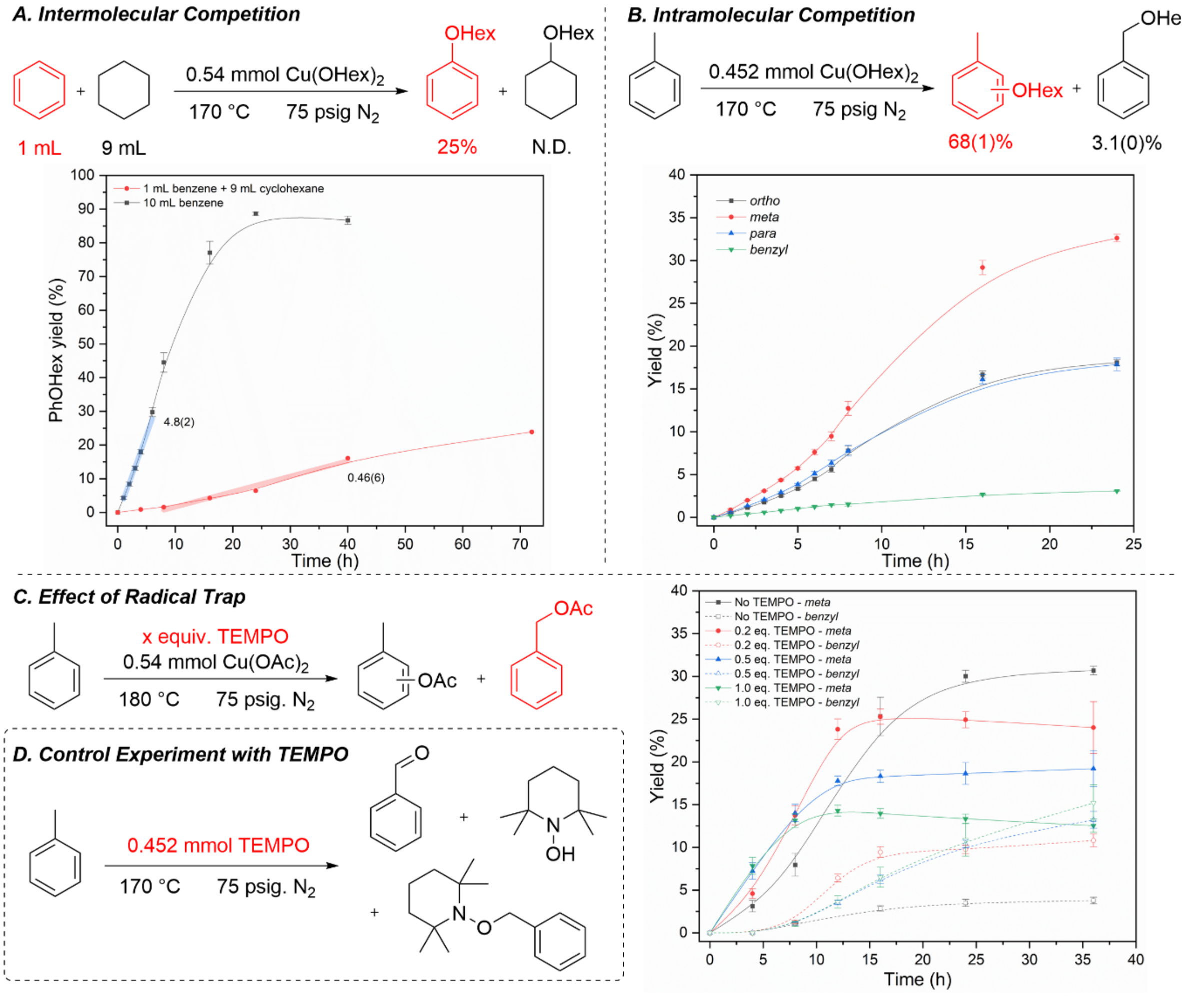

Figure 2. Differentiate between radical and non-radical pathways. (**A**) Intermolecular competition of sp^2 vs. sp^3 C–H bonds using a mixture of benzene and cyclohexane. N.D. = not detected. (**B**) Intermolecular competition of sp^2 vs. sp^3 C–H bonds using toluene. (**C**) meta-Tolyl acetate and benzyl acetate yield versus time plot of reaction using different amount of (2,2,6,6-tetramethylpiperidin-1-yl)oxyl (TEMPO). Reaction conditions: toluene (10 mL, 94.1 mmol), $Cu(OAc)_2$, (98 mg, 0.540 mmol), TEMPO (0, 0.2, 0.5, and 1.0 equiv. relative to $Cu(OAc)_2$), 75 psig N_2, 180 °C. (**D**) Observed products of control experiment using TEMPO with no Cu(II) salt. Reaction conditions: toluene (10 mL, 94.1 mmol), TEMPO (71 mg, 0.452 mmol), 75 psig N_2, 170 °C. Standard deviations were calculated from at least three independent experiments.

In the presence of 1 atm of dried O_2, the selectivity of toluene acetoxylation reaction using $Cu(OAc)_2$ changed to form benzyl acetate (**Table 2**, entry 3), which is evidence for a radical process since the weaker benzyl C–H bond was functionalized. Also, the inclusion of O_2

suppresses reactivity with the stronger sp^2 tolyl C–H bonds, similar to our observation when using benzene as the substrate that exhibited lower yield in the presence of O_2 (**Table 1**, entry 4). The selectivity shifts from sp^2 C–H bond functionalization to benzylic functionalization is expected since mixing Cu(II) with O_2 is known to form Cu–peroxo and/or superoxo species (*39-42*), which likely leads to the formation of free radical species that favor weaker sp^3 C–H bond functionalization over stronger sp^2 C–H bonds. Since hexamethylbenzene (HMB), which has been used as the standard for GC analysis, contains benzylic C–H bonds and the Cu(II) mediated functionalization of toluene activates benzyl C–H bonds under some conditions, control experiments were done using $Cu(OAc)_2$ and toluene as the substrate at 180 °C with *in situ and ex situ* addition of HMB for GC-FID analysis (Figure S6). As expected, under anaerobic conditions, the consumption of HMB is negligible, while under aerobic conditions a competing radical-based reaction with HMB was observed, which is consistent with our proposal that reaction pathways are distinct under anaerobic versus aerobic conditions. Therefore, to avoid complications caused by the consumption of HMB, all the reported quantifications used *ex situ* addition of HMB for GC analysis. Water was also examined as an additive (**Table 2**, entries 4 and 11), and similar to O_2, the presence of 1 equivalent of water (relative to Cu) switches the reaction selectivity for toluene activation towards benzylic C–H functionalization although tolyl products are still observed (Supplementary Materials, Section 11). We suspect that water coordinates to $Cu_2(\mu\text{-}OAc)_4$ to form copper(II) acetate hydrate, $Cu_2(\mu\text{-}OAc)_4{\cdot}2H_2O$, which can convert to monomeric $Cu(OAc)_2{\cdot}(H_2O)_n$ (*43*) or other decomposition species such as Cu/Cu_2O under reaction temperatures that could lead to a radical process(es) that competes with the organometallic Cu(II)-mediated pathway. The observation of a similar change in reaction selectivity using commercial copper(II) acetate monohydrate [$Cu_2(\mu\text{-}OAc)_4{\cdot}2H_2O$] (**Table 2**, entry 5) is consistent with the observation of reactions with water added to anhydrous $Cu_2(\mu\text{-}OAc)_4$. The addition of increasing amounts of carboxylic acid (**Table 2**, entries 6 and 12–14) decreases the reaction rate without changing the benzyl-to-tolyl selectivity. This suggests that carboxylic acid inhibits the organometallic reaction pathway but does not facilitate undesirable radical-based processes, which is different from the effect of water or O_2.

Table 2. Selected results for toluene acetoxylation and related reactions using simple Cu(II) salts. Yield of the tolyl or benzyl carboxylate is relative to the limiting reagent (CuX_2). Reaction conditions: toluene (10 mL, 94.1 mmol), CuX_2 (for $Cu(OAc)_2$, 0.57 mol%, 0.540 mmol; for $Cu(OPiv)_2$ or $Cu(OHex)_2$, 0.48 mol%, 0.452 mmol), 75 psig N_2. CuX_2 = $Cu(OAc)_2$ anhydrous, $Cu(OPiv)_2$, or $Cu(OHex)_2$. Standard deviations were calculated from at least three independent experiments

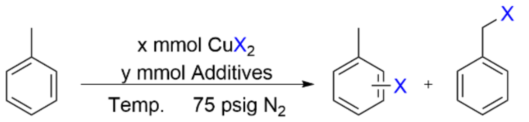

Entry	CuX_2	Temp. (°C)	Additive (equiv.)	Yield (%)					Time (h)
				Total	Benzyl	Para	Meta	Ortho	
1	$Cu(OAc)_2$	180	none	72(1)	4.0(5)	19(0)	31(1)	18(0)	40
2	$Cu(OAc)_2$	170	none	71(2)	5.0(2)	20(1)	31(1)	15(1)	96
3[a]	$Cu(OAc)_2$	180	Dried O_2	95(6)	89(6)	1(0)	3(0)	2(0)	4
4	$Cu(OAc)_2$	180	H_2O (1.0)	37(2)	17(2)	5(0)	10(0)	5(0)	40
5	$Cu(OAc)_2{\cdot}H_2O$	180	none	48(3)	23(0)	7(1)	13(2)	6(1)	96

6	$Cu(OAc)_2$	180	HOAc (1.0)	50(3)	3.0(3)	12(1)	23(2)	11(1)	40
7	$Cu(OAc)_2$	180	Ac_2O (1.0)	3(1)	0.3(0)	1(0)	2(0)	1(0)	24
8	$Cu(OPiv)_2$	170	none	33(0)	0.9(1)	10(0)	16(0)	7(0)	16
9	$Cu(OHex)_2$	180	none	54(1)	2.4(2)	16(0)	24(0)	12(0)	8
10	$Cu(OHex)_2$	170	none	72(0)	3.1(1)	18(1)	33(1)	18(0)	24
11	$Cu(OHex)_2$	170	H_2O (1.0)	41(3)	8.4(0)	9(1)	16(2)	7(1)	24
12	$Cu(OHex)_2$	170	HOHex (1.0)	68(2)	2.9(1)	19(1)	33(1)	13(0)	40
13	$Cu(OHex)_2$	170	HOHex (2.0)	56(1)	2.8(3)	15(0)	28(1)	10(3)	40
14	$Cu(OHex)_2$	170	HOHex (4.0)	36(1)	2.3(2)	10(0)	19(1)	6(1)	48

[a] Using 1 atm of dried O_2, the total top pressure of O_2 and N_2 is 75 psig.

The presence of bi- or tridentate ligand (e.g., bipyridine, terpyridine, tetramethyl ethylenediamine, 1,2-bis(dimethylphosphino)ethane.) shuts down the benzene functionalization reaction, and many ligands result in a switch of the reaction selectivity for toluene activation towards benzylic C–H functionalization (Supplementary Materials, Section 5.1). However, using $(MeO)_3P{=}O$, which we presume is a weakly coordinating ligand, only slows down the arene functionalization process without changing the sp^2-to-sp^3 selectivity (**Figure 3A**). By refluxing $Cu(OAc)_2$ and $(MeO)_3P{=}O$ in toluene, the resulting product was found to be the bis-Cu complex $\{(MeO)_3P{=}O\}_2Cu_2(\mu\text{-}OAc)_4$. The structure of $\{(MeO)_3P{=}O\}_2Cu_2(\mu\text{-}OAc)_4$ was confirmed by a single crystal X-ray diffraction study (**Figure 3B**). We speculate that $(MeO)_3P{=}O$ does not disrupt the dimeric Cu(II) structure and, hence, only slows down the functionalization of arenes by competing with the arene substrate for Cu coordination. In contrast, multi-dentate ligands likely convert bis-Cu(II) to monomeric Cu(II) complexes of the type $LCu^{II}X_2$ that are not active for the functionalization of arenes (**Figure 4A**). By monitoring the initial rate of the reaction using different amounts of soluble $Cu_2(\mu\text{-}OHex)_4$ and 2-ethylhexanoic acid (HOHex), the reaction was found to be first-order in $Cu_2(\mu\text{-}OHex)_4$ concentration (**Figure S26**) and inverse first-order in HOHex concentration (**Figure S29**). Based on these observations, we propose a plausible reaction pathway and rate equation (**Figure 4B**). Reversible arene C–H activation by $Cu_2(\mu\text{-}X)_4$ (X = OAc, OHex or OPiv) and dissociation of carboxylic acid is followed by an overall rate limiting reductive coupling/elimination of aryl ester. This proposed reaction pathway is consistent with the results of DFT calculations (see below).

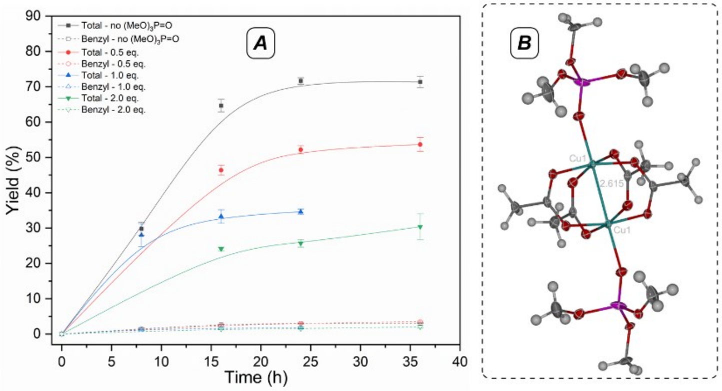

Figure 3. Effects of weakly coordinating $(MeO)_3P{=}O$ ligands. (**A**) Sum of tolyl/benzyl 2-ethylhexanoate yields and benzyl 2-ethylhexanoate yield versus time plot with the presence of different amounts of $(MeO)_3P{=}O$ ligands. Reaction conditions: toluene (10 mL, 94.1 mmol), $Cu(OHex)_2$, 0.48 mol%, 0.452 mmol), $(MeO)_3P{=}O$ (0, 0.5, 1.0, and 2.0 equiv. relative to

$Cu(OHex)_2$), 75 psig N_2, 170 °C. Standard deviations were calculated from at least three independent experiments. (**B**) ORTEP of $\{(MeO)_3P{=}O\}_2Cu_2(\mu\text{-}OAc)_4$. Ellipsoids are drawn at 50% probability level.

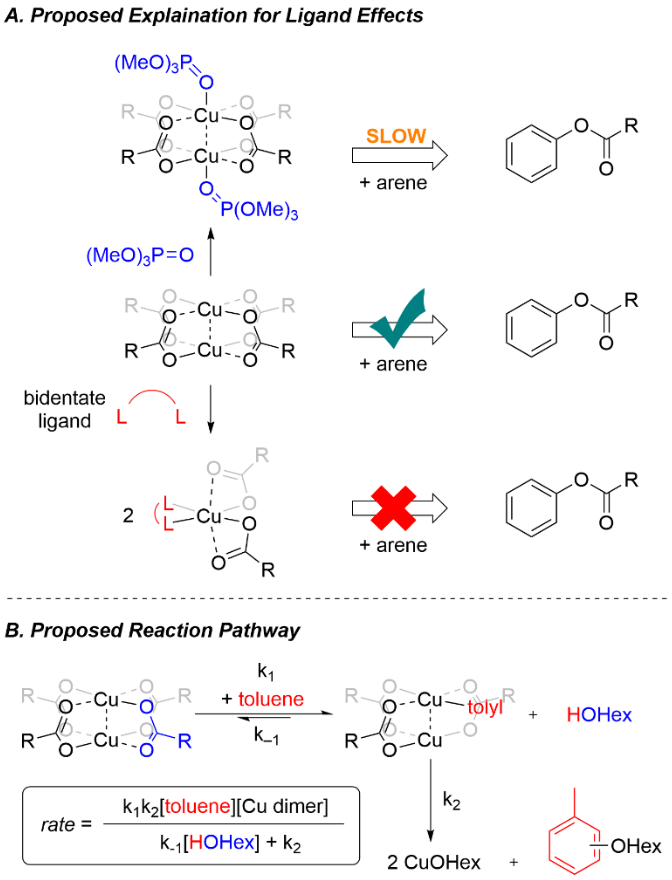

Figure 4. Ligand effects and reaction pathway. (**A**) Proposed competing pathway in the arene acetoxylation reaction in the presence of weakly coordinating or bidentate ligand. (**B**) Proposed reaction pathway and associated rate law.

Based on the proposed rate equation (**Figure 4B**), the rate constant for the C–H activation step (k_1) can be calculated via a curve fitting of *rate* versus [HOHex] (**Figure 5C**) or the intercept from a 1/*rate* versus [HOHex] plot (**Figure S31**), where *rate* is the slope of the concentration of tolyl 2-ethylhexanoate versus time plot (**Figure S28**). Both plots gave good fits, which is consistent with the proposed reaction pathway. The rate constant for the C–H activation step (k_1) and the related activation free energy ($\Delta G_1^{\ddagger}{}_{443K}$) can be estimated from the intercept as 2.7(4) 10^{-6} $s^{-1}\cdot M^{-1}$ and 38(1) kcal·mol^{-1} (Supplementary Materials, Section 9). A slight induction period was observed for all of the Cu(II)-mediated acetoxylation reactions without addition of carboxylic acid. The reaction rate of the induction period and the initial linear region were monitored at different reaction temperatures using soluble $Cu(OHex)_2$ with toluene as the substrate (**Figure S23**, **Table S11**). It was found that a decrease in reaction temperature led to an increase in the induction period, and at 180 °C, there is no observable induction period. The induction period of the reaction was also studied in the presence of variable concentrations of HOHex (**Figure S24**), and with the addition of more acid, the induction period becomes less obvious. We propose that the induction period is due to the process of dissolving Cu(II) salt under acid free conditions.

To gain insight into the Cu(II)-mediated arene C–H activation step, we studied the kinetic isotope effect (KIE) using C_6H_6 and C_6D_6 as the substates with soluble $Cu(OHex)_2$ at 170 °C. The KIE value was determined to be 3.0(1) for parallel reactions using benzene and benzene-*d*$_6$, and 2.8(1) for the intermolecular competition reactions using a mixture of benzene and benzene-*d*$_6$ with a 1-to-1 molar ratio (**Figure 5A**). This type of KIE has typically been interpreted as C–H cleavage that occurs during or before the rate-determining step (*44-45*), which is consistent with the proposed reaction pathway (**Figure 4B**). In the presence of 8 equivalents of DOAc (relevant to $Cu(OAc)_2$), a small amount of deuterium incorporation (3.0(3)%) was found in the product (**Figure 5B**), which likely indicates that the C–H activation step is partially reversible and is also consistent with the proposed reaction pathway (**Figure 4B**).

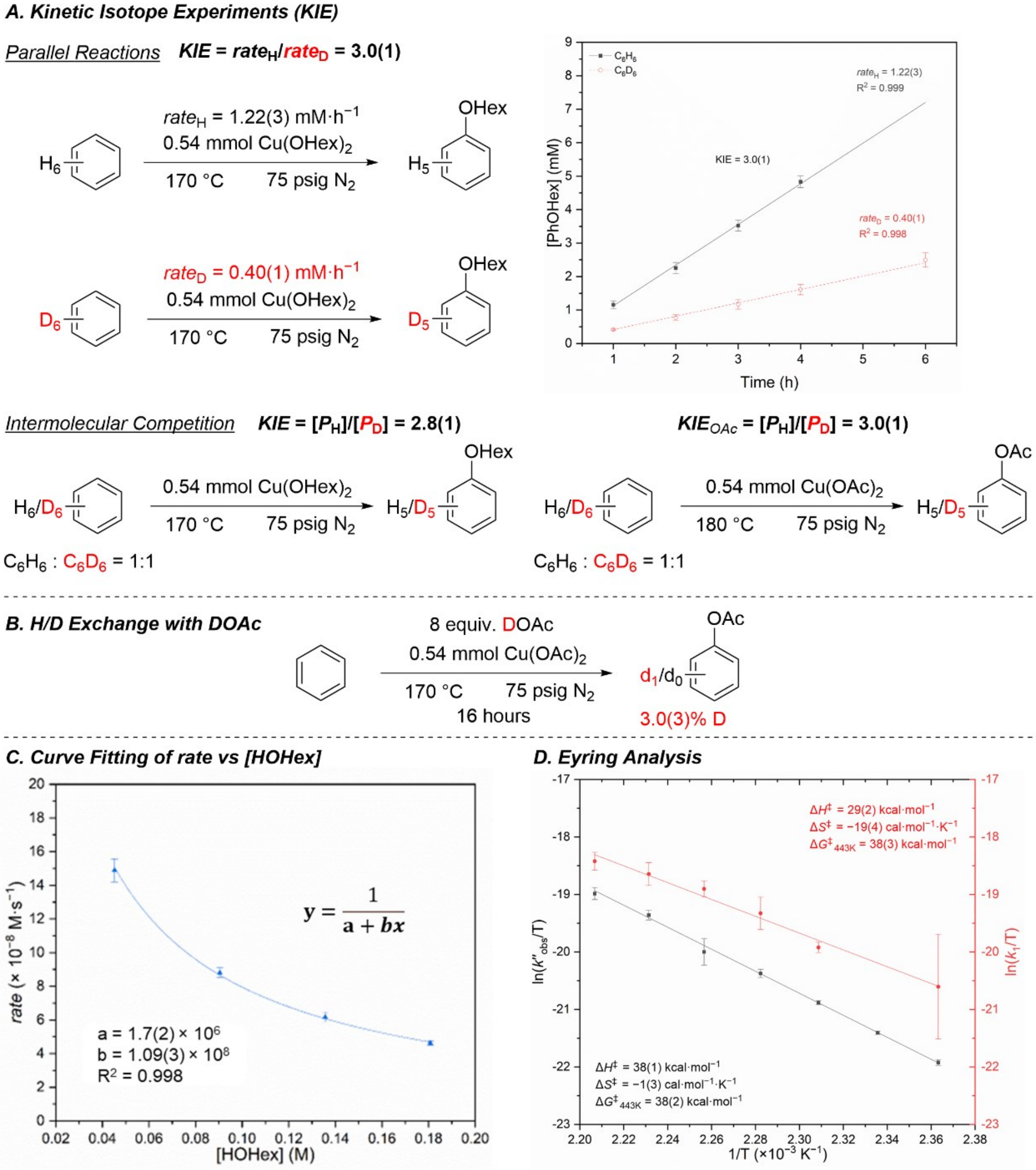

Figure 5. Mechanistic Studies. (**A**) Measurements of kinetic isotope effect (KIE) using parallel reactions and intermolecular competition experiments. (**B**) H/D exchange experiment using acetic acid-*d*$_1$ (DOAc) as the deuterium source. (**C**) Curve fitting of observed reaction rates (*rate*) versus

HOHex concentration plot for 2-ethylhexanoation of toluene using $Cu(OHex)_2$ with the addition of different amounts of HOHex at 170 °C. (**D**) Eyring plot for toluene functionalization using $Cu(OHex)_2$ calculated with k_{obs} (in black) and k_1 (in red). Reaction rates were measured for production of tolyl 2-ethylhexanoate over the temperature range 150 – 180 °C under the conditions with addition of variant amounts of 2-ethylhexanoic acid. Rate equation: $rate = k''_{obs}$[toluene][Cu dimer]. The rate constant k_1 was calculated using curve fitting of observed reaction rates versus HOHex concentration.

An Eyring analysis was performed using reaction rates measured at seven temperatures between 150 and 180 °C (**Figure 5D**, in black), which provided an activation enthalpy ($\Delta H^{\ddagger}$) of 38(1) $kcal{\cdot}mol^{-1}$. The activation entropy ($\Delta S^{\ddagger}$) was found to be –1(3) $cal{\cdot}mol^{-1}{\cdot}K^{-1}$ assuming an overall second order rate law ($rate = k''_{obs}$[toluene][$Cu_2(\mu\text{-}OHex)_4$]), which indicates that the entropy has a negligible effect on the overall reaction. The small entropy of activation is potentially due to the use of excess toluene as the solvent and/or that the C–H activation step may only be partially rate limiting (see DFT calculations below). Using an Arrhenius plot (**Figure S47**), the activation energy (E_a) was determined to be 39(1) $kcal{\cdot}mol^{-1}$. As described above, the rate constant of the C–H activation step (k_1) can be determined, therefore, a set of reaction have been done over the temperature range 150 – 180 °C under the conditions with addition of variant amounts of 2-ethylhexanoic acid in order to calculate k_1 at different temperatures (**Table S25**). The Eyring analysis performed using k_1 at different temperatures as it shown in **Figure 5D** (in red), and these data indicate a $\Delta H^{\ddagger}$ of 29(2) $kcal{\cdot}mol^{-1}$ and a $\Delta S^{\ddagger}$ of –19(4) $cal{\cdot}mol^{-1}{\cdot}K^{-1}$. These activation parameters are consistent with the proposed mechanism for arene C–H activation and the results of computational modeling (see below).

Computational modeling. To further understand the reaction mechanism, we used DFT and TD-DFT calculations to examine closed-shell (C–H activation) and open-shell (e.g., electron transfer, hydrogen atom transfer, and proton-coupled electron transfer; Supplementary Materials, Section 16) reaction pathways. Both dinuclear $Cu_2(\mu\text{-}OAc)_4$ and mononuclear $Cu(OAc)_2$ models were examined for each pathway. **Figure 6** presents unrestricted MN15L (*46*) functional results. This method was chosen based on its general accuracy for thermodynamics, barriers, and spin states for first-row transition metals. While there are no overall different mechanistic conclusions using alternative functionals {e.g., M06L (*47*)} and wavefunction methods {DLPNO-CCSD(T) (*48-49*)}, the relative energies of structures do change (see Supplementary Materials, Section for comparison **Table S36**).

Using the results of DFT calculations in combination with our experimental results (see above and Supplementary Materials), we propose the reaction mechanism outlined by the calculated energy landscape for the para position of toluene shown in **Figure 6A** (in black). In an initial step, $Cu_2(\mu\text{-}OAc)_4$ (**1**) coordinates and activates a C–H bond of toluene (we modeled the para C–H bond) in a one-step metalation process to form (*p*-tolyl)Cu^{II}(HOAc)(μ-OAc)$_2Cu^{II}$(κ^2-OAc) (**2**) with a calculated Gibbs activation energy of 41.4 $kcal{\cdot}mol^{-1}$ (at 170 °C). This C–H activation step involves concerted formation of the Cu–*p*-tolyl bond with simultaneous proton transfer to the acetate ligand in a pathway (**TS1**). The structure **TS1** shown in **Figure 6A** is similar to many other transition states reported for arene C–H activation by metal acetate complexes and is often called concerted metalation deprotonation (*50*). The energies for **TS1** at the ortho and meta positions of toluene are very similar (within 1.6 $kcal{\cdot}mol^{-1}$ or closer) to the transition state energy for para C–H activation, which is consistent with the very small experimental selectivity (see **Figure 6B**).

Dissociation of HOAc precedes C–O reductive coupling between tolyl and acetate ligands (**TS2**), which occurs with a calculated Gibbs activation energy of 39.2 kcal·mol^{-1} and forms (tolyl acetate)$Cu_2(\mu\text{-}OAc)_2$ (**5**). **TS2** has a typical 3-centered reductive coupling/elimination geometry where the Cu–OAc and Cu–Ar bonds are broken with simultaneous formation of the new C–O bond. Dissociation of the tolyl acetate from **5** gives the final organic product. Inspection of structure and bonding after HOAc dissociation and during the reductive elimination step suggests that this process occurs through a Cu(III)/Cu(I) intermediate rather than a Cu(II)/Cu(II) intermediate. This leads us to conclude that the second Cu atom is important to facilitating the C–O reductive coupling step by an intramolecular oxidation, a proposal that is consistent with calculated energetics using the monomeric $Cu(OAc)_2$ (**7**) species (see below and **Figure 6A** in blue).

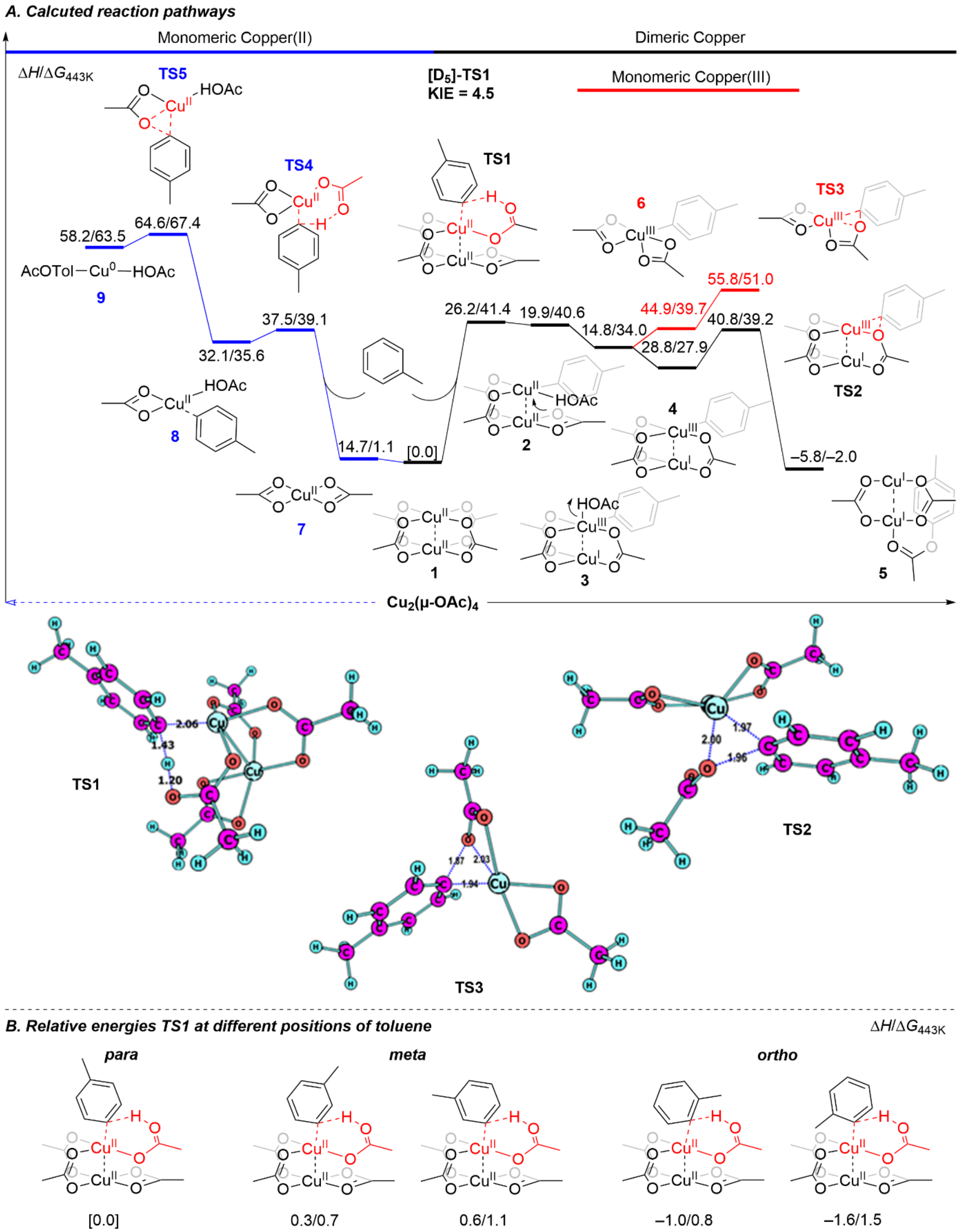

Figure 6. Computational modeling of possible reaction pathways. (**A**) UMN15L/Def2-TZVPP//UMN15L/Def2-SVP Calculated relative enthalpies and free energies (in kcal·mol^{-1}) at 170 °C of the calculated reaction pathways with $Cu_2(\mu\text{-}OAc)_4$ and $Cu(OAc)_2$ monomer. (**B**) Relative energies of ortho, para, and meta C–H activation transition states.

Figure 6A also shows a comparison of the dinuclear Cu pathway to arene activation by monomeric $Cu(OAc)_2$ (**7**), which is potentially viable because the Gibbs energy for formation of the monomer only requires 1.1 kcal·mol^{-1} relative to $Cu_2(\mu\text{-}OAc)_4$ (**1**). While the toluene C–H activation by monomeric $Cu(OAc)_2$ (**7**) has a Gibbs activation barrier close to the experimental value (39.1 kcal·mol^{-1}), the calculated barrier (67.4 kcal·mol^{-1}) for the C–O reductive coupling step is too high to be feasible. Therefore, a mononuclear Cu pathway would require conversion of the mononuclear Cu–*p*-tolyl (**8**) to a dinuclear structure for reductive elimination or aryl acetate product formation. However, the low concentration of the mononuclear Cu–*p*-tolyl structure (**8**), is because it is highly endothermic, which makes this set of reaction steps unlikely. Another possible reaction pathway is C–H activation by $Cu(OAc)_2$ (**7**) followed by an intermolecular disproportionation to form a monomeric Cu(III) species **6** along with a Cu(I) compound, which avoids the high energy aryl ester reductive elimination from the Cu(II) intermediate **8** (see above). The disproportionation pathway is similar to the previously proposed mechanism for directed Cu(II)-mediated C–H acetoxylation/hydroxylation (*13,16*). However, the calculated activation barrier for C–O reductive coupling from the monomeric Cu(III)–tolyl intermediate via **TS3** (51.0 kcal·mol^{-1},) indicates this is an uncompetitive pathway. Also, if the reaction undergoes the intermolecular disproportionation route, the addition of 0.5 equivalents of ligand (e.g., bipyridine, tetramethyl ethylenediamine, etc.) might be expected to accelerate the reaction since the donor ligand could facilitate the oxidation of LCu(II)–tolyl to form the monomeric LCu(III)–tolyl intermediate; however, our data shows that all ligands studied inhibit the $Cu_2(\mu\text{-}OAc)_4$ mediated organometallic arene functionalization.

The calculated activation enthalpy and Gibbs energies for the dinuclear Cu C–H activation step ($\Delta H^‡$ = 26.2 kcal·mol^{-1}, $\Delta G^‡_{443K}$ = 41.4 kcal·mol^{-1}) are consistent with the experimental values from the Eyring analysis using k_1 ($\Delta H^‡$ = 29(2) kcal·mol^{-1}, $\Delta G^‡_{443K}$ = 38(3) kcal·mol^{-1}). The calculated KIE for the C–H(D) activation transition state using deuterium at all five aromatic positions and corresponding zero-point energies is 4.5, which is slightly larger than but still consistent with the experimental KIE value of ~3.0, especially considering that zero-point energy is only one of several factors that control KIE values. Also, the KIE study was measured based on the overall *rate* of the reaction, instead of the individual rate constant k_1. The reductive coupling/elimination step has energies of $\Delta H^‡$ = 40.8 kcal·mol^{-1} and $\Delta G^‡_{443K}$ = 39.2 kcal·mol^{-1}. The nearly equal energies for C–H activation and reductive elimination suggests that both transition states may control the reaction rate and one transition state may dominate under specific conditions. This viewpoint provides an explanation for the observed primary KIE value, partially reversible C–H activation step, and possible overall rate limiting reductive elimination with a small activation entropy. We propose that the C–H activation step is reversible, therefore, at low acid concentrations the equilibrium of the C–H activation step may contribute to the isotope effect. There are several possible reasons for a very small activation entropy, one possible origin is provided by the energy landscape. **Figure 6A** shows that the Gibbs energy for the reductive elimination transition state ($\Delta H^‡$ = 40.8 kcal·mol^{-1}, $\Delta G^‡_{443K}$ = 39.2 kcal·mol^{-1}) is very close to the barrier for C–H activation. This could be explained by a scenario where C–H activation as well as HOAc dissociation and reductive elimination steps all contribute to control the reaction rate. This proposal is also consistent with the experimentally observed difference in $\Delta S^‡$ when performing the Eyring analysis using k_{obs} and k_1 as well as the inverse first order dependence of the reaction rate on acid concentration.

In addition to the mononuclear and dinuclear C–H activation reaction pathways outlined in **Figure 6**, we also examined several other possible mechanisms for toluene C–H functionalization that are much less likely based on calculated energies. While details of these pathways are presented in the Supplementary Materials, it is useful to mention a few key alternative pathways. For example, outersphere single-electron transfer from toluene to Cu(II) requires > 140 kcal·mol^{-1} since Cu(II) is only a moderate oxidant and the resulting charged species are not significantly stabilized in toluene solvent. Also, we estimated innersphere one-electron transfer from the toluene π system to the Cu metal center using time-dependent (TD) DFT excitation energies calculated from the Cu–toluene π-coordination complex (**Figure 7**). This excitation energy is 36.9 kcal/mol and the orbitals responsible for this excitation are shown in **Figure 7** (π-orbital **70β** to the Cu orbital **71β**). While this excitation may be competitive with **TS1**, subsequent C–H activation from this excited state still require about 39.6 kcal·mol^{-1} and therefore an overall barrier of > 60 kcal·mol^{-1} (for alternative pathways, see Supplementary Materials for details), which suggests that electron transfer chemistry is not occurring. We also considered reactions that proceed through the initial formation of radical species, such as ·OH or ·OAc. However, these pathways are unlikely based on calculated Gibbs energies, which require 52.8 kcal·mol^{-1} and 60.5 kcal·mol^{-1}, respectively, to form these radical species from the initial Cu complex.

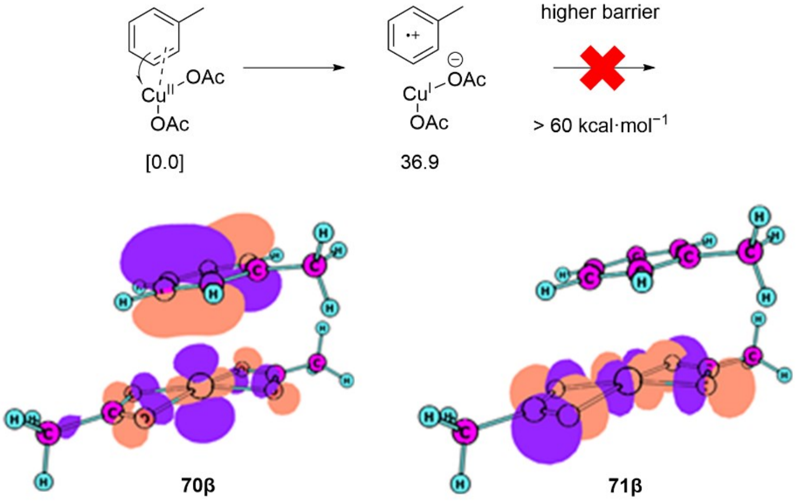

Figure 7. Computational modeling of single-electron transfer pathways. UMN15L/Def2-TZVPP//MN15L/Def2-SVP Calculated energies for TD-DFT estimation for excitation between occupied orbital **70β** (toluene centered) to unoccupied orbital **71β** (Cu centered).

Isolation of products and recycling of Cu(II). The reaction using Cu(OHex)$_2$ was scaled to 1.1 g where 78% isolated yield of PhOHex and 83% recovery of the Cu(OHex)$_2$ were achieved (**Figure 8A**). We demonstrated recycling of the recovered Cu(OHex)$_2$ using toluene as the substrate, and no difference in tolyl-to-benzyl selectivity was observed upon use of the recycled Cu(OHex)$_2$ (Supplementary Materials, Section 17.1). PhOAc can also be isolated with 69% yield along with 93% recovery of the used Cu(OAc)$_2$. With knowledge of the effect of molecular sieves, water and O$_2$ (Supplementary Materials, Sections 10–12), we pursued a demonstration that the Cu(II) salt could be recovered and recycled after a completed reaction, similar in some ways to one version of the commercialized Wacker process (*32-35*). To do so, after each reaction, 0.5 equivalents of HOHex was added to the reaction solution and stirred under air until the solution turned dark blue indicating that Cu(I) is oxidized to Cu(II). Then 3Å molecular sieves were added to remove the generated water that was formed from the regeneration of Cu(OHex)$_2$. After filtration to remove the sieves and trapped water, $Cu(OHex)_2$ was isolated and reused for the reaction under anaerobic conditions and demonstrated a similar rate as before either using benzene or toluene as the substrate (**Figure 8B**), and 2.5 TOs (based on bis-Cu not monomeric Cu) of PhOHex can be achieved. The hydrolysis step of the phenyl carboxylate products was performed (Supplementary Materials, Section 21) using a previously reported procedure (*51*). In addition, phenol can be formed in > 95% yield by reacting MeOH with phenyl carboxylate product, so that the formed methyl ester and remaining MeOH can be readily isolated from the reaction mixture by distillation. Overall, in the recycle experiments, 240% total yield from benzene to phenol was achieved {based on Cu(II)} with 0.6% total conversion of the initial benzene. By changing the molar ratio of benzene and Cu(II) salts along with using solvent, 2.4% conversion of benzene can be reached, however, there is likely a thermodynamic inhibition to achieving higher conversion (Supplementary Materials, Section 22).

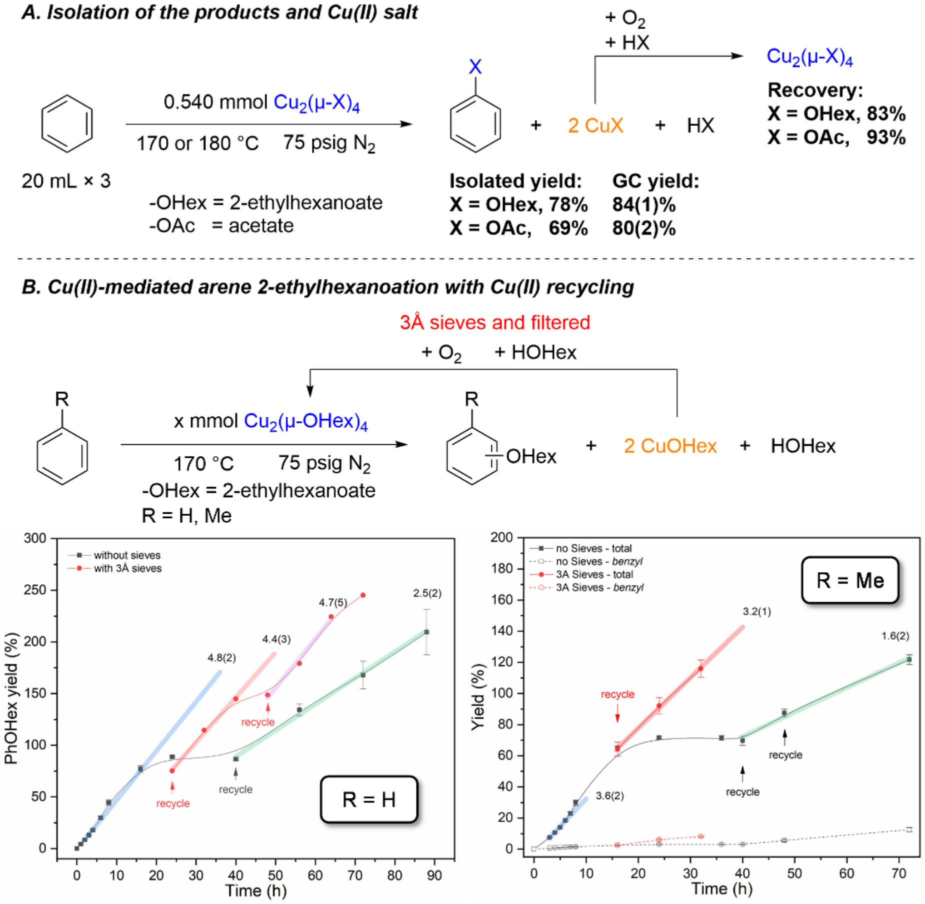

Figure 8. Isolation of products and extension to Cu(II) recycling. (**A**) Isolation of the phenyl 2-ethylhexanoate/acetate product and recovery of the $Cu_2(\mu\text{-}X)_4$ used in the reaction. Reaction conditions: benzene (20 mL, 224.6 mmol), $Cu_2(\mu\text{-}X)_4$ (0.24 mol% 0.540 mmol, $Cu_2(\mu\text{-}OAc)_4$ 196 mg; $Cu_2(\mu\text{-}OHex)_4$ 378 mg), under 75 psig N_2 at 180 °C for $Cu_2(\mu\text{-}OAc)_4$; 170 °C for $Cu_2(\mu\text{-}OHex)_4$. (**B**) Cu(II)-mediated arene 2-ethylhexanoation with Cu(II) recycling. Reaction conditions: for benzene (10 mL, 112.3 mmol), $Cu_2(\mu\text{-}OHex)_4$ (189 mg, 0.270 mmol), 75 psig N_2, 170 °C; for toluene (10 mL, 94.1 mmol), $Cu_2(\mu\text{-}OHex)_4$ (158 mg, 0.226 mmol), 75 psig N_2, 170 °C. Yield of the phenyl carboxylate is relative to the limiting Cu reagent. Standard deviations were calculated from at least three independent experiments.

Discussion

We report a process using copper(II) carboxylate salts to oxidize benzene and toluene without installation of a directing group through a proposed organometallic Cu(II)-mediated C–H activation pathway. While Cu-mediated C–H activation to form intermediates with Cu–C bonds have been proposed previously (*13,15*), to our knowledge, evidence for non-radical Cu-mediated functionalization of hydrocarbons with strong C–H bonds is rare. Further, we have demonstrated that the copper(II) carboxylate salts used for the reaction can be isolated, recycled, and reused for the reaction with little change in reactivity, which is similar to one version of the commercial Wacker process for ethylene oxidation (*32-35*). Regeneration of the copper(II) carboxylate salt is achieved in solution using O_2 after each reaction, and with the removal of the generated water, the reaction maintains a similar rate using recycle Cu(II) (Supplementary Materials, Section 20). By adding a hydrolysis step of the phenyl carboxylate product, which is a known reaction (*51*), this process could provide a coproduct-free synthetic route for phenol production using cheap air-recyclable Cu(II) salts.

Our experimental and computational mechanistic studies demonstrate that the dimeric Cu(II) structure of $Cu_2(\mu\text{-}OAc)_4$ lowers the activation barrier for the product forming C–O reductive coupling step from the Cu(III)–Ar intermediate. This proposal shares some similarities to our previously published catalysis for styrene production using benzene and ethylene for which we propose the incorporation of Cu(II) in a Rh/Cu/Rh structure reduces the activation barrier for an O–H bond forming reductive coupling step (*52*). Thus, the incorporation of a Lewis acidic and oxidizing Cu(II) center (and possibly related metals) into a multi-metallic species might represent a general strategy to facilitate catalytic hydrocarbon oxidation.

Materials and Methods

General Considerations. All reactions were performed under a dinitrogen atmosphere using Schlenk line techniques or inside a dinitrogen filled glovebox unless specified otherwise. GC-FID was performed using a Shimadzu GC-2014 system with a 30 m × 0.25 mm DB-5ms capillary column with 0.25 μm film thickness. GC-MS was performed using a Shimadzu GCMS-QP2010 Plus or a Shimadzu GCMS-QP2020 NX with a 30 m × 0.25 mm capillary column with Rxi-5ms with 0.25 μm film thickness using electron impact ionization method. Toluene was dried using sodium-benzophenone/ketyl stills under dinitrogen atmosphere and stored inside the glovebox. Methanol was dried using a calcium hydride still under dinitrogen atmosphere and stored inside a glovebox. Benzene, acetonitrile, and methylene chloride were dried using a solvent purification system with activated alumina. Toluene-d_8, acetonitrile-d_3, benzene-d_6, and methylene chloride-d_2 were dried and stored over activated 3Å molecular sieves inside a glovebox. Except for the Cu(II) salts (see below), all other chemicals were purchased from commercial sources and used as received. Elemental analyses were performed by the University of Virginia Chemistry Department Elemental Analysis Facility.

General Procedures for Pretreatment of Cu(II) Salts. The commercial Cu(II) salts was ground and heated in a Schlenk flask under ~10 mTorr vacuum in a 110 °C oil bath for at least 1 day or 90 °C for 3 days. During the drying process, the condensation of a colorless liquid was observed on the side of the round bottom flask, and a heat gun was used to completely transfer the liquid into the liquid dinitrogen trap on the Schlenk line. After drying, the needle valve was sealed and the flask containing Cu(II) salts was directly transferred into the glovebox without opening to air. **Alternate method to purify $Cu(OHex)_2$.** Commercial $Cu(OHex)_2$ (10 g) was dissolved in 60 mL of EtOH and stirred until a homogeneous solution was formed. Then deionized water was added until no more precipitation. The mixture was filtered to collect the fine greenish-blue solid. After washing with water a few times, the solid was placed in a vacuum oven at 100 °C until no mass change to yield the final product (9.3 g). This method particularly useful for removing high boiling point 2-ehtylhexanoic acid in the commercial Cu(OHex)$_2$. For more details, please see Supplementary Materials Section 2.3.

Synthesis of Copper(II) 2-ethylhexanoate (Cu(OHex)$_2$). To a solution of NaOH (10 g, 250 mmol) in 300 mL of EtOH, 2-ethylhexanoate acid (42 mL, 263 mmol) was added and stirred for 2 hours at room temperature. Then, Cu(NO$_3$)$_2$·3H$_2$O (30.2 g, 125 mmol) was added to the solution. The color of the solution was blue and then changed to a greenish-blue color with solid precipitation. The mixture was then stirred at room temperature for at least 2 hours, then deionized water was added to precipitate out the solid product as a greenish-blue fine solid. The solid was washed with deionized water to remove the water-soluble salts. Then the solid product was placed in a vacuum oven heated to 100–110 °C under vacuum until no mass changes to yield the final Cu(OHex)$_2$ product (39.4 g, 90% isolated yield). The solid can be further dried using the same procedure described above, but can also be used directly without further drying process.

Synthesis of (MeO)$_3$P=O Cu(OAc)$_2$. To a solution of Cu(OAc)$_2$ (100 mg, 0.551 mmol) in 5 mL of toluene, trimethyl phosphate (1 mL, 8.639 mmol) and 1 mL of HOAc were added. After heating at reflux for approximately 1 hour, the suspension was filtered hot to remove the undissolved Cu(OAc)$_2$ (most of the Cu(OAc)$_2$ was not dissolved), and crystals suitable for X-ray analysis were obtained by slow evaporation from light-blue filtrate (20 mg, 11% isolated yield). Anal. Calcd for $C_{14}H_{30}O_{16}P_2Cu_2$: C, 26.13; H, 4.70. Found: trial#1 C, 25.84; H, 4.48.; trial#2 C, 25.92; H, 4.49.

Synthesis of (MeO)$_3$P=O Cu(OPiv)$_2$. To a solution of Cu(OPiv)$_2$ (100 mg, 0.389 mmol) in 5 mL of toluene, trimethyl phosphate (45 µL, 0.389 mmol) was added. After heating at reflux for approximately 1 hour, the solution was filtered hot, and crystals suitable for X-ray analysis were obtained from slow evaporation from the blue filtrate (82 mg, 53% isolated yield). Anal. Calcd for $C_{26}H_{54}P_2O_{16}Cu_2$: C, 38.47; H, 6.71. Found: C, 38.53; H, 6.96.

General procedure for Cu(II)-mediated arene C–H acetoxylation. Under an atmosphere of dry dinitrogen inside a glovebox that the purity was maintained as $O_2 < 5$ ppm, and $H_2O < 1$ ppm, the copper(II) salt {CuX$_2$, X = OAc, 0.540 mmol (0.48 mol% to relative to benzene, 0.57 mol% relative to toluene); for soluble CuX$_2$, X = OPiv or OHex, 0.48 mol% relative to arene (0.540 mmol for reaction using benzene; 0.452 mmol for reaction using toluene)} was added into a dried Andrews Glass Lab-Crest Fisher-Porter tube with a stir bar, then 10 mL of arene (benzene or toluene) was measured by a syringe and added to the reaction tube. The Fisher-Porter tube was then sealed and pressurized with 75 psig of dinitrogen. Then the mixture was stirred in an oil bath at reaction temperature (the oil bath temperature was confirmed by an external mercury thermometer), and the stir plate stirring speed was set to 550 rpm. The reaction time was recorded starting at the time the oil bath temperature reached the setting point, which typically required 5–10 mins after placing the Fisher-Porter tube into the 1 L oil bath with 500 – 600 mL of silicone oil (usable range from −40 to 200 °C). The reaction was monitored periodically by taking a 100 µL aliquot of the reaction solution and mixing with 100 µL of a hexamethylbenzene (HMB) stock solution in arene (benzene or toluene) with known HMB concentration, then quickly washing the mixture with saturated sodium hydroxide solution (~0.2 mL). The resulting organic layer was subjected to GC-FID and/or GC-MS for quantitative analysis, using relative peak areas versus HMB as the standard.

References

1. R. J. Schmidt, Industrial catalytic processes—phenol production. *Appl. Catal. A-Gen.* **280**, 89-103 (2005). doi: 10.1016/j.apcata.2004.08.030
2. A. Mancuso, O. Sacco, D. Sannino, *et al.*, One-Step Catalytic or Photocatalytic Oxidation of Benzene to Phenol: Possible Alternative Routes for Phenol Synthesis? *Catalysts* **10**, 1424 (2020). doi: 10.3390/catal10121424
3. K. H. Kuechler, F. M. Benitez Dehydrogenation processes and phenol compositions. U.S. Patent 9,242,918, Jan. 26, 2016.
4. H. Nair, C. L. Becker, R. A. Sothen, *et al.* Process for producing phenol. U.S. Patent 9,233,890, Jan 12, 2016.
5. W. D. McGhee Selective introduction of active sites for hydroxylation of benzene. U.S. Patent 5,977,008, Nov. 2, 1999.
6. H. Orita, T. Hayakawa, M. Shimizu, *et al.*, Catalytic hydroxylation of benzene by the copper-ascorbic acid-O2 system. *J. Mol. Catal.* **42**, 99-103 (1987). doi: 10.1016/0304-5102(87)85043-5
7. T. Kitamura, H. Kanzaki, R. Hamada, *et al.*, Liquid-phase oxidation of benzene to phenol by copper catalysts in aqueous solvent with a high acetic acid concentration. *Can. J. Chem.* **82**, 1597-1605 (2004). doi: 10.1139/v04-123
8. A. Häusser, M. Trautmann, E. Roduner, Spin trapping of hydroxyl radicals on Cu/HY zeolites suspended in aqueous solution. *Chem. Commun.* **47**, 6954-6956 (2011). doi: 10.1039/C1CC11181G
9. D. Wang, J. N. Jaworski, S. S. Stahl, Pd-Catalyzed Aerobic Oxidation Reactions: Industrial Applications and New Developments. in *Liquid Phase Aerobic Oxidation Catalysis: Industrial Applications and Academic Perspectives*, Stahl, S. S.; Alsters, P. L., Eds. (Wiley-VCH, Weinheim, 2016), pp 113-138.
10. S. R. Neufeldt, M. S. Sanford, Controlling Site Selectivity in Palladium-Catalyzed C–H Bond Functionalization. *Acc. Chem. Res.* **45**, 936-946 (2012). doi: 10.1021/ar300014f
11. T. Yoneyama, R. H. Crabtree, Pd(II) catalyzed acetoxylation of arenes with iodosyl acetate. *J. Mol. Catal. A: Chem.* **108**, 35-40 (1996). doi: 10.1016/1381-1169(95)00289-8
12. X. Chen, X.-S. Hao, C. E. Goodhue, *et al.*, Cu(II)-Catalyzed Functionalizations of Aryl C−H Bonds Using O2 as an Oxidant. *J. Am. Chem. Soc.* **128**, 6790-6791 (2006). doi: 10.1021/ja061715q
13. X. Li, Y.-H. Liu, W.-J. Gu, *et al.*, Copper-Mediated Hydroxylation of Arenes and Heteroarenes Directed by a Removable Bidentate Auxiliary. *Org. Lett.* **16**, 3904-3907 (2014). doi: 10.1021/ol5016064
14. B. K. Singh, R. Jana, Ligand-Enabled, Copper-Promoted Regio- and Chemoselective Hydroxylation of Arenes, Aryl Halides, and Aryl Methyl Ethers. *J. Org. Chem.* **81**, 831-841 (2016). doi: 10.1021/acs.joc.5b02302
15. S.-Z. Sun, M. Shang, H.-L. Wang, *et al.*, Cu(II)-Mediated C(sp2)–H Hydroxylation. *J. Org. Chem.* **80**, 8843-8848 (2015). doi: 10.1021/acs.joc.5b01351
16. A. M. Suess, M. Z. Ertem, C. J. Cramer, *et al.*, Divergence between Organometallic and Single-Electron-Transfer Mechanisms in Copper(II)-Mediated Aerobic C–H Oxidation. *J. Am. Chem. Soc.* **135**, 9797-9804 (2013). doi: 10.1021/ja4026424
17. J. Gallardo-Donaire, R. Martin, Cu-Catalyzed Mild C(sp2)–H Functionalization Assisted by Carboxylic Acids en Route to Hydroxylated Arenes. *J. Am. Chem. Soc.* **135**, 9350-9353 (2013). doi: 10.1021/ja4047894

18. W. Wang, F. Luo, S. Zhang, *et al.*, Copper(II)-Catalyzed Ortho-Acyloxylation of the 2-Arylpyridines sp2 C−H Bonds with Anhydrides, Using O2 as Terminal Oxidant. *J. Org. Chem.* **75**, 2415-2418 (2010). doi: 10.1021/jo1000719

19. M. Shang, Q. Shao, S.-Z. Sun, *et al.*, Identification of monodentate oxazoline as a ligand for copper-promoted ortho-C–H hydroxylation and amination. *Chem. Sci.* **8**, 1469-1473 (2017). doi: 10.1039/C6SC03383K

20. X. Wu, Y. Zhao, H. Ge, Pyridine-enabled copper-promoted cross dehydrogenative coupling of C(sp2)–H and unactivated C(sp3)–H bonds. *Chem. Sci.* **6**, 5978-5983 (2015). doi: 10.1039/C5SC02143J

21. X. Zeng, W. Yan, M. Paeth, *et al.*, Copper-Catalyzed, Chloroamide-Directed Benzylic C–H Difluoromethylation. *J. Am. Chem. Soc.* **141**, 19941-19949 (2019). doi: 10.1021/jacs.9b11549

22. D. K. Pandey, A. B. Shabade, B. Punji, Copper-Catalyzed Direct Arylation of Indoles and Related (Hetero)arenes: A Ligandless and Solvent-free Approach. *Adv. Synth. Catal.*, (2020). doi: 10.1002/adsc.202000312

23. R. Odani, K. Hirano, T. Satoh, *et al.*, Copper-Mediated Formally Dehydrative Biaryl Coupling of Azine N-Oxides and Oxazoles. *J. Org. Chem.* **80**, 2384-2391 (2015). doi: 10.1021/acs.joc.5b00037

24. M. Nishino, K. Hirano, T. Satoh, *et al.*, Copper-Mediated and Copper-Catalyzed Cross-Coupling of Indoles and 1,3-Azoles: Double C–H Activation. *Angew. Chem. Int. Ed.* **51**, 6993-6997 (2012). doi: 10.1002/anie.201201491

25. K. Takamatsu, Y. Hayashi, S. Kawauchi, *et al.*, Copper-Catalyzed Regioselective C–H Amination of Phenol Derivatives with Assistance of Phenanthroline-Based Bidentate Auxiliary. *ACS Catal.* **9**, 5336-5344 (2019). doi: 10.1021/acscatal.9b01145

26. M. Shang, S.-Z. Sun, H.-X. Dai, *et al.*, Cu(OAc)2-Catalyzed Coupling of Aromatic C–H Bonds with Arylboron Reagents. *Org. Lett.* **16**, 5666-5669 (2014). doi: 10.1021/ol5027377

27. C. Yamamoto, K. Takamatsu, K. Hirano, *et al.*, Copper-Catalyzed Intramolecular Benzylic C–H Amination for the Synthesis of Isoindolinones. *J. Org. Chem.* **81**, 7675-7684 (2016). doi: 10.1021/acs.joc.6b01393

28. M. Shang, S.-Z. Sun, H.-L. Wang, *et al.*, Exceedingly Fast Copper(II)-Promoted ortho C–H Trifluoromethylation of Arenes using TMSCF3. *Angew. Chem. Int. Ed.* **53**, 10439-10442 (2014). doi: 10.1002/anie.201404822

29. X. Wu, J. Miao, Y. Li, *et al.*, Copper-promoted site-selective carbonylation of sp3 and sp2 C–H bonds with nitromethane. *Chem. Sci.* **7**, 5260-5264 (2016). doi: 10.1039/C6SC01087C

30. R. Wang, Y. Li, R.-X. Jin, *et al.*, Copper-catalyzed oxidative C(sp3)–H/C(sp2)–H cross-coupling en route to carbocyclic rings. *Chem. Sci.* **8**, 3838-3842 (2017). doi: 10.1039/C7SC00250E

31. J. Wang, R. Sang, X. Chong, *et al.*, Copper-catalyzed radical cascade oxyalkylation of olefinic amides with simple alkanes: highly efficient access to benzoxazines. *Chem. Commun.* **53**, 7961-7964 (2017). doi: 10.1039/C7CC04213B

32. J. A. Keith, P. M. Henry, The Mechanism of the Wacker Reaction: A Tale of Two Hydroxypalladations. *Angew. Chem. Int. Ed.* **48**, 9038-9049 (2009). doi: 10.1002/anie.200902194

33. J. Smidt, W. Hafner, R. Jira, *et al.*, Katalytische Umsetzungen von Olefinen an Platinmetall-Verbindungen Das Consortium-Verfahren zur Herstellung von Acetaldehyd. *Angew. Chem.* **71**, 176-182 (1959). doi: 10.1002/ange.19590710503

34. G. F. M. Eckert, R. Jira, H. M. Bolt, K. Golka, , in *Ullmann's Encyclopedia of Industrial Chemistry*, (Wiley-VCH Verlag, Weinheim, Germany,, 2000), pp 1-17.

35. Hoechst Reveals Wacker Process Details. *Chem. Eng. News Archive* **39**, 52-55 (1961). doi: 10.1021/cen-v039n016.p052

36. J. Chen, R. J. Nielsen, W. A. Goddard*, et al.*, Catalytic Synthesis of Superlinear Alkenyl Arenes Using a Rh(I) Catalyst Supported by a "Capping Arene" Ligand: Access to Aerobic Catalysis. *J. Am. Chem. Soc.* **140**, 17007-17018 (2018). doi: 10.1021/jacs.8b07728

37. F. Kong, S. Gu, C. Liu*, et al.*, Effects of Additives on Catalytic Arene C–H Activation: Study of Rh Catalysts Supported by Bis-phosphine Pincer Ligands. *Organometallics* **39**, 3918-3935 (2020). doi: 10.1021/acs.organomet.0c00623

38. D. Munz, M. Webster-Gardiner, R. Fu*, et al.*, Proton or Metal? The H/D Exchange of Arenes in Acidic Solvents. *ACS Catal.* **5**, 769-775 (2015). doi: 10.1021/cs501620f

39. C. E. Elwell, N. L. Gagnon, B. D. Neisen*, et al.*, Copper–Oxygen Complexes Revisited: Structures, Spectroscopy, and Reactivity. *Chem. Rev.* **117**, 2059-2107 (2017). doi: 10.1021/acs.chemrev.6b00636

40. L. M. Mirica, X. Ottenwaelder, T. D. P. Stack, Structure and Spectroscopy of Copper−Dioxygen Complexes. *Chem. Rev.* **104**, 1013-1046 (2004). doi: 10.1021/cr020632z

41. E. A. Lewis, W. B. Tolman, Reactivity of Dioxygen−Copper Systems. *Chem. Rev.* **104**, 1047-1076 (2004). doi: 10.1021/cr020633r

42. A. Conde, L. Vilella, D. Balcells*, et al.*, Introducing Copper as Catalyst for Oxidative Alkane Dehydrogenation. *J. Am. Chem. Soc.* **135**, 3887-3896 (2013). doi: 10.1021/ja310866k

43. P. Sharrock, M. Melník, Copper(II) acetates: from dimer to monomer. *Can. J. Chem.* **63**, 52-56 (1985). doi: 10.1139/v85-009

44. E. M. Simmons, J. F. Hartwig, On the Interpretation of Deuterium Kinetic Isotope Effects in C–H Bond Functionalizations by Transition-Metal Complexes. *Angew. Chem. Int. Ed.* **51**, 3066-3072 (2012). doi: 10.1002/anie.201107334

45. W. D. Jones, Isotope Effects in C−H Bond Activation Reactions by Transition Metals. *Acc. Chem. Res.* **36**, 140-146 (2003). doi: 10.1021/ar020148i

46. H. S. Yu, X. He, D. G. Truhlar, MN15-L: A New Local Exchange-Correlation Functional for Kohn–Sham Density Functional Theory with Broad Accuracy for Atoms, Molecules, and Solids. *J. Chem. Theory Comput.* **12**, 1280-1293 (2016). doi: 10.1021/acs.jctc.5b01082

47. Y. Zhao, D. G. Truhlar, A new local density functional for main-group thermochemistry, transition metal bonding, thermochemical kinetics, and noncovalent interactions. *J. Chem. Phys.* **125**, 194101 (2006). doi: 10.1063/1.2370993

48. C. Riplinger, B. Sandhoefer, A. Hansen*, et al.*, Natural triple excitations in local coupled cluster calculations with pair natural orbitals. *J. Chem. Phys.* **139**, 134101 (2013). doi: 10.1063/1.4821834

49. C. Riplinger, F. Neese, An efficient and near linear scaling pair natural orbital based local coupled cluster method. *J. Chem. Phys.* **138**, 034106 (2013). doi: 10.1063/1.4773581

50. D. L. Davies, S. A. Macgregor, C. L. McMullin, Computational Studies of Carboxylate-Assisted C–H Activation and Functionalization at Group 8–10 Transition Metal Centers. *Chem. Rev.* **117**, 8649-8709 (2017). doi: 10.1021/acs.chemrev.6b00839

51. W. Medina-Ramos, M. A. Mojica, E. D. Cope*, et al.*, Water at elevated temperatures (WET): reactant, catalyst, and solvent in the selective hydrolysis of protecting groups. *Green Chem.* **16**, 2147-2155 (2014). doi: 10.1039/C3GC42569J

52. C. B. Musgrave, W. Zhu, N. Coutard*, et al.*, Mechanistic Studies of Styrene Production from Benzene and Ethylene Using [(η2-C2H4)2Rh(μ-OAc)]2 as Catalyst Precursor: Identification

of a Bis-RhI Mono-CuII Complex As the Catalyst. *ACS Catal.* **11**, 5688-5702 (2021). doi: 10.1021/acscatal.1c01203

53. G. R. Fulmer, A. J. M. Miller, N. H. Sherden*, et al.*, NMR Chemical Shifts of Trace Impurities: Common Laboratory Solvents, Organics, and Gases in Deuterated Solvents Relevant to the Organometallic Chemist. *Organometallics* **29**, 2176-2179 (2010). doi: 10.1021/om100106e

54. L.-H. Xie, M. P. Suh, Flexible Metal–Organic Framework with Hydrophobic Pores. *Chem. Eur. J.* **17**, 13653-13656 (2011). doi: 10.1002/chem.201103078

55. D. S. Schrage, D. C. Malarik, A novel quartz dendritic growth chamber for low temperature microgravity experimentation. *Rev. Sci. Instrum.* **70**, 4624-4633 (1999). doi: 10.1063/1.1150124

56. A. Bruylants, M. Tits, C. Dieu*, et al.*, Directed chlorination. II. Aliphatic acids and nitriles, alkyl acetates. *Bull. Soc. Chim. Belg.* **61**, 366-92 (1952). doi:

57. J. G. Traynham, M. A. Battiste, Solvolyses of Some Sterically Hindered Aliphatic Esters1. *J. Org. Chem.* **22**, 1551-1554 (1957). doi: 10.1021/jo01363a004

58. P. A. Levene, F. A. Taylor, ON OXIDATION OF TERTIARY HYDROCARBONS. *J. Biol. Chem.* **54**, 351-362 (1922). doi: 10.1016/S0021-9258(18)85747-7

59. A. L. J. Beckwith, Reactions of Alkoxy Radicals. I. The Reactions of Di-tert.-butyl Peroxide with n-Butyric Acid and Ethyl n-Butyrate. *Aust. J. Chem.* **13**, 244-255 (1960). doi:

60. S. Bette, A. Costes, R. K. Kremer*, et al.*, On Verdigris, Part III: Crystal Structure, Magnetic and Spectral Properties of Anhydrous Copper(II) Acetate, a Paddle Wheel Chain. *Z. Anorg. Allg. Chem.* **645**, 988-997 (2019). doi: 10.1002/zaac.201900125

61. E. O. Pentsak, D. B. Eremin, E. G. Gordeev*, et al.*, Phantom Reactivity in Organic and Catalytic Reactions as a Consequence of Microscale Destruction and Contamination-Trapping Effects of Magnetic Stir Bars. *ACS Catal.* **9**, 3070-3081 (2019). doi: 10.1021/acscatal.9b00294

62. T. Jintoku, K. Takaki, Y. Fujiwara*, et al.*, Palladium Catalyzed Direct Oxidation of Benzene with Molecular Oxygen to Phenol. *Bull. Chem. Soc. Jpn.* **63**, 438-441 (1990). doi: 10.1246/bcsj.63.438

63. M. Okamoto, T. Yamaji, A Selective Synthesis of Biphenyl by the Pd(Oac)2/MoO2(acac)2/O2/AcOH Catalyst System. *Chem. Lett.* **30**, 212-213 (2001). doi: 10.1246/cl.2001.212

64. A. R. Dick, K. L. Hull, M. S. Sanford, A Highly Selective Catalytic Method for the Oxidative Functionalization of C−H Bonds. *J. Am. Chem. Soc.* **126**, 2300-2301 (2004). doi: 10.1021/ja031543m

65. L. V. Desai, K. J. Stowers, M. S. Sanford, Insights into Directing Group Ability in Palladium-Catalyzed C−H Bond Functionalization. *J. Am. Chem. Soc.* **130**, 13285-13293 (2008). doi: 10.1021/ja8045519

66. N. R. Deprez, M. S. Sanford, Synthetic and Mechanistic Studies of Pd-Catalyzed C−H Arylation with Diaryliodonium Salts: Evidence for a Bimetallic High Oxidation State Pd Intermediate. *J. Am. Chem. Soc.* **131**, 11234-11241 (2009). doi: 10.1021/ja904116k

67. D. C. Powers, M. A. L. Geibel, J. E. M. N. Klein*, et al.*, Bimetallic Palladium Catalysis: Direct Observation of Pd(III)−Pd(III) Intermediates. *J. Am. Chem. Soc.* **131**, 17050-17051 (2009). doi: 10.1021/ja906935c

68. J. M. Racowski, A. R. Dick, M. S. Sanford, Detailed Study of C−O and C−C Bond-Forming Reductive Elimination from Stable C2N2O2−Ligated Palladium(IV) Complexes. *J. Am. Chem. Soc.* **131**, 10974-10983 (2009). doi: 10.1021/ja9014474

69. K. J. Stowers, M. S. Sanford, Mechanistic Comparison between Pd-Catalyzed Ligand-Directed C−H Chlorination and C−H Acetoxylation. *Org. Lett.* **11**, 4584-4587 (2009). doi: 10.1021/ol901820w

70. D. C. Powers, D. Y. Xiao, M. A. L. Geibel, *et al.*, On the Mechanism of Palladium-Catalyzed Aromatic C−H Oxidation. *J. Am. Chem. Soc.* **132**, 14530-14536 (2010). doi: 10.1021/ja1054274

71. M. H. Emmert, A. K. Cook, Y. J. Xie, *et al.*, Remarkably High Reactivity of Pd(OAc)2/Pyridine Catalysts: Nondirected C□H Oxygenation of Arenes. *Angew. Chem. Int. Ed.* **50**, 9409-9412 (2011). doi: 10.1002/anie.201103327

72. J. Pei, S. Qin, G.-y. Li, *et al.*, Water-promoted One-step Anodic Acetoxylation of Benzene to Phenyl Acetate with High Selectivity. *Chin. J. Chem. Phys.* **24**, 244-248 (2011). doi: 10.1088/1674-0068/24/02/244-248

73. N. Wang, T. M. McCormick, S.-B. Ko, *et al.*, PtII and PdII Complexes with a trans-Chelating Bis(pyridyl) Ligand. *Eur. J. Inorg. Chem.* **2012**, 4463-4469 (2012). doi: 10.1002/ejic.201200442

74. A. K. Cook, M. H. Emmert, M. S. Sanford, Steric Control of Site Selectivity in the Pd-Catalyzed C–H Acetoxylation of Simple Arenes. *Org. Lett.* **15**, 5428-5431 (2013). doi: 10.1021/ol4024248

75. J. B. Gary, A. K. Cook, M. S. Sanford, Palladium Catalysts Containing Pyridinium-Substituted Pyridine Ligands for the C–H Oxygenation of Benzene with K2S2O8. *ACS Catal.* **3**, 700-703 (2013). doi: 10.1021/cs300786j

76. A. K. Cook, M. S. Sanford, Mechanism of the Palladium-Catalyzed Arene C–H Acetoxylation: A Comparison of Catalysts and Ligand Effects. *J. Am. Chem. Soc.* **137**, 3109-3118 (2015). doi: 10.1021/jacs.5b00238

77. S. P. Desai, M. Mondal, J. Choudhury, Chelating Bis-N-heterocyclic Carbene–Palladium(II) Complexes for Oxidative Arene C–H Functionalization. *Organometallics* **34**, 2731-2736 (2015). doi: 10.1021/om501163m

78. S. L. Zultanski, S. S. Stahl, Palladium-catalyzed aerobic acetoxylation of benzene using NOx-based redox mediators. *J. Organomet. Chem.* **793**, 263-268 (2015). doi: 10.1016/j.jorganchem.2015.03.003

79. H. M. D. Bandara, D. Jin, M. A. Mantell, *et al.*, Non-directed aromatic C–H amination: catalytic and mechanistic studies enabled by Pd catalyst and reagent design. *Catal. Sci. Technol.* **6**, 5304-5310 (2016). doi: 10.1039/C6CY00457A

80. L. Li, Y. Wang, T. Yang, *et al.*, Palladium-catalyzed non-directed CH benzoxylation of simple arenes with iodobenzene dibenzoates. *Tetrahedron Lett.* **57**, 5859-5863 (2016). doi: 10.1016/j.tetlet.2016.11.055

81. C. Valderas, K. Naksomboon, M. Á. Fernández-Ibáñez, Ligand-Promoted Palladium-Catalyzed C−H Acetoxylation of Simple Arenes. *ChemCatChem* **8**, 3213-3217 (2016). doi: 10.1002/cctc.201600757

82. M. H. Majeed, P. Shayesteh, L. R. Wallenberg, *et al.*, Polymer-Supported Palladium(II) Carbene Complexes: Catalytic Activity, Recyclability, and Selectivity in C−H Acetoxylation of Arenes. *Chem. Eur. J.* **23**, 8457-8465 (2017). doi: 10.1002/chem.201700777

83. K. Naksomboon, C. Valderas, M. Gómez-Martínez, *et al.*, S,O-Ligand-Promoted Palladium-Catalyzed C–H Functionalization Reactions of Nondirected Arenes. *ACS Catal.* **7**, 6342-6346 (2017). doi: 10.1021/acscatal.7b02356

84. A. Shrestha, M. Lee, A. L. Dunn*, et al.*, Palladium-Catalyzed C–H Bond Acetoxylation via Electrochemical Oxidation. *Org. Lett.* **20**, 204-207 (2018). doi: 10.1021/acs.orglett.7b03559
85. D. Lapointe, K. Fagnou, Overview of the Mechanistic Work on the Concerted Metallation–Deprotonation Pathway. *Chem. Lett.* **39**, 1118-1126 (2010). doi: 10.1246/cl.2010.1118
86. M. J. Frisch, G. W. Trucks, H. B. Schlegel*, et al. Gaussian 16 Rev. C.01*, Wallingford, CT, 2016.
87. F. Weigend, R. Ahlrichs, Balanced basis sets of split valence, triple zeta valence and quadruple zeta valence quality for H to Rn: Design and assessment of accuracy. *PCCP* **7**, 3297-3305 (2005). doi: 10.1039/B508541A
88. F. Weigend, Accurate Coulomb-fitting basis sets for H to Rn. *PCCP* **8**, 1057-1065 (2006). doi: 10.1039/B515623H
89. J. Zheng, X. Xu, D. G. Truhlar, Minimally augmented Karlsruhe basis sets. *Theor. Chem. Acc.* **128**, 295-305 (2011). doi: 10.1007/s00214-010-0846-z
90. F. Neese, Software update: the ORCA program system, version 4.0. *WIREs Comput. Mol. Sci.* **8**, e1327 (2018). doi: 10.1002/wcms.1327
91. R. L. Carlin, *Magnetochemistry*. Springer Berlin Heidelberg: 1986. *pp*. 77–82. *ISBN 978-3642707353*.
92. J. Pipek, P. G. Mezey, A fast intrinsic localization procedure applicable for ab initio and semiempirical linear combination of atomic orbital wave functions. *J. Chem. Phys.* **90**, 4916-4926 (1989). doi: 10.1063/1.456588
93. T. Lu, F. Chen, Multiwfn: A multifunctional wavefunction analyzer. *J. Comput. Chem.* **33**, 580-592 (2012). doi: 10.1002/jcc.22885
94. Y. Kanazawa, T. Mitsudome, H. Takaya*, et al.*, Pd/Cu-Catalyzed Dehydrogenative Coupling of Dimethyl Phthalate: Synchrotron Radiation Sheds Light on the Cu Cycle Mechanism. *ACS Catal.* **10**, 5909-5919 (2020). doi: 10.1021/acscatal.0c00918
95. V. R. Yatham, W. Harnying, D. Kootz*, et al.*, 1,4-Bis-Dipp/Mes-1,2,4-Triazolylidenes: Carbene Catalysts That Efficiently Overcome Steric Hindrance in the Redox Esterification of α- and β-Substituted α,β-Enals. *J. Am. Chem. Soc.* **138**, 2670-2677 (2016). doi: 10.1021/jacs.5b11796
96. W. Harnying, P. Sudkaow, A. Biswas*, et al.*, N-Heterocyclic Carbene/Carboxylic Acid Co-Catalysis Enables Oxidative Esterification of Demanding Aldehydes/Enals, at Low Catalyst Loading. *Angew. Chem. Int. Ed.* **60**, 19631-19636 (2021). doi: 10.1002/anie.202104712
97. N. Moszner, J. Angermann, U. Fischer*, et al.*, Methacrylated Calix[6]arenes as Low Shrinking Additives for Dental Restorative Composites. *Macromolecular Materials and Engineering* **296**, 937-943 (2011). doi: 10.1002/mame.201100021
98. C. B. Rao, B. Chinnababu, Y. Venkateswarlu, An Efficient Protocol for Alcohol Protection Under Solvent- and Catalyst-Free Conditions. *J. Org. Chem.* **74**, 8856-8858 (2009). doi: 10.1021/jo901374k
99. K. W. Quasdorf, X. Tian, N. K. Garg, Cross-Coupling Reactions of Aryl Pivalates with Boronic Acids. *J. Am. Chem. Soc.* **130**, 14422-14423 (2008). doi: 10.1021/ja806244b
100. T. Liu, X. Shao, Y. Wu*, et al.*, Highly Selective Trifluoromethylation of 1,3-Disubstituted Arenes through Iridium-Catalyzed Arene Borylation. *Angew. Chem. Int. Ed.* **51**, 540-543 (2012). doi: 10.1002/anie.201106673
101. W. M. Czaplik, S. Grupe, M. Mayer*, et al.*, Practical iron-catalyzed dehalogenation of aryl halides. *Chem. Commun.* **46**, 6350-6352 (2010). doi: 10.1039/C0CC01980A
102. Bruker *Saint; SADABS; APEX3.*, Bruker AXS Inc.: Madison, Wisconsin, USA., 2012.

103. G. M. Sheldrick, SHELXT - integrated space-group and crystal-structure determination. *Acta Crystallogr. A: Found. Adv.* **A71**, 3-8 (2015). doi: 10.1107/s2053273314026370

104. O. Dolomanov, L. Bourhis, R. Gildea*, et al.*, OLEX2: A complete structure solution, refinement and analysis program. *J. Appl. Cryst.* **42**, 339-341 (2009). doi: 10.1107/S0021889808042726

105. G. Sheldrick *CELL_NOW*, Version 2008/4; Georg-August-Universität Göttingen: Göttingen, Germany, 2008.

106. A. Singh, A. Tiwari, S. M. Mahajani, R. D. Gudi, *Ind. Eng. Chem. Res.* **45**, 2017-2025 (2006). doi: 10.1021/ie0505514

Acknowledgments

We thank Xiaofan Jia for assistance with GC-MS analysis for the KIE studies and Ke Zhang for assistance with statistical analysis. We thank Shen-Wei Yu for assistance with ICP-OES analysis. We thank Brigham Young University and the Office of Research Computing, especially the Fulton Supercomputing Lab.

Funding

Experimental works was supported by the U.S. National Science Foundation under award CHE-2102433. Computational work was supported by the U.S. National Science Foundation Chemical Catalysis (CAT) Program under award CHE-2153215.

Author contributions

Conceptualization: TBG conceived the project.

Methodology: TBG and FK designed the experiments. DHE and SC designed the computational simulations. JC performed preliminary experimental designs.

Investigation: FK performed the experiments and analyzed experimental data with the help from CL, DAD. JC performed preliminary experimental studies. DE and SC provided computational simulation. WZ performed an experiment to isolate a single-crystal of Cu(OPiv)$_2$.

Funding acquisition: TBG, DHE

Supervision: TBG, DHE, SZ, WS

Writing – original draft: FK, SC

Writing – review & editing: TBG, DHE, FK, SC, DAD, JC, CL, and WZ.

Competing interests

Authors declare that they have no competing interests.

Data and materials availability

All data are available in the main text or the supplementary materials.

Supplementary Materials

Materials and Methods
Supplementary Text
Figs. S1 to S92
Tables S1 to S36
NMR Spectra

HRMS Spectra
References (*53–106*)
Crystallographic Information File